

DESIGNING HIGH-PERFORMANCE MICRO-PUMPS BASED ON NO-MOVING-PARTS VALVES

Ron L. Bardell[†] Nigel R. Sharma[‡] Fred K. Forster^{*†}

Martin A. Afromowitz[‡] Robert J. Penney[†]

[†]Department of Mechanical Engineering

[‡]Department of Electrical Engineering

University of Washington

Seattle, Washington 98195

ABSTRACT

Micro-pumps utilizing no-moving-parts (NMP) valves, driven by a piezoelectric element bonded to a flexible membrane have been developed by a number of research groups (Olsson et al, 1995a; Forster et al, 1995; Gerlach and Wurmus, 1995). Recently, pump heads of over 7 m of H₂O have been achieved (Olsson et al, 1996). However, no systematic methods have been reported that predict pump performance and guide the design of optimally performing pumps. We have developed a linearized dynamic system model that provides a detailed understanding of the relationship between a realistic set of system parameters and pump performance. These parameters include flow characteristics of the NMP valves, characteristics of the working fluid, pump geometry, and materials used in fabrication. Utilization of the model as a design tool, resulted in a dramatic improvement from previous "flexible" pump designs with maximum heads of approximately 0.24 m of H₂O to a "stiff" design with a maximum head of 4.75 m of H₂O, a twenty-fold increase in performance. Corresponding flow rates increased from 85 to 750 μ l/min, a nine-fold increase.

Q	Volume flow rate
R	Resistance
V	Driving voltage on piezoelectric element
\hat{V}	Volume
W_c	Membrane centerline deflection
\dot{W}_c	Membrane centerline velocity
d_H	Hydraulic diameter
f_e	Membrane centerline deflection per volt
h	Height
k	Membrane stiffness
m	Effective mass of membrane, see Eq. (6)
n	Ratio of specific heats
r_o	Radius of membrane
w_v	Width of valve channel
γ	Shape factor of membrane
μ	Absolute viscosity
ω, ω_n	Radian frequency, resonance
ρ	Density of fluid
$()_a ()_w$	Subscript for fluid: air or water
$()_c ()_v ()_t$	Subscript for component: chamber, valve, or tubing

NOMENCLATURE

A	Area of membrane
C	Capacitance
I	Inertance
K	Bulk Modulus of working fluid
L	Length of channel
P	Fluid pressure, gage
ΔP	Pressure drop across valve

INTRODUCTION

Micropumps with no-moving-parts (NMP) valves are of interest because of their simplicity, ease of manufacture, and the ability to pass particles. The valve efficiency can be characterized by its diodicity, the ratio of the pressure drop across the valve in reverse flow to that in forward flow. Typically, these pumps are actuated by a piezoelectric disk bonded to a membrane covering the pump chamber

*Direct correspondence to forster@u.washington.edu

as shown in Fig. 1. The inlet and outlet are connected to the circular pump chamber by NMP valves. To achieve high performance, such a pump is operated at a system resonance. A simplified theoretical analysis of resonance frequency was discussed by Olsson (1995b) that considered the elastic properties of the membrane and the fluid inertia in the valve, but other dominant parameters, such as pump chamber capacitance, were neglected. To design a pump to operate at optimal resonant frequency and amplitude, a more complete system model is invaluable.

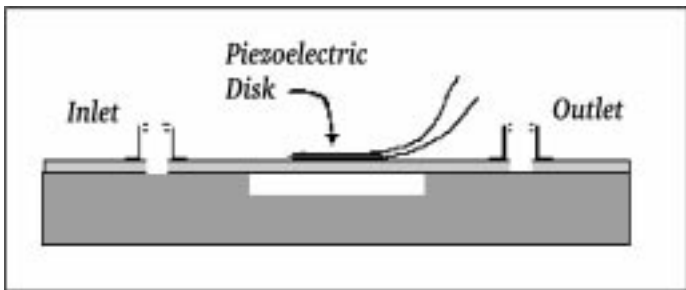


FIGURE 1: EDGE VIEW OF A MICRO-PUMP ACTUATED BY A PIEZOELECTRIC DISK BONDED TO THE PUMP MEMBRANE.

A linear frequency-domain model has been developed that predicts the frequency response of the complete system given the characteristics of the pump components and the pump load. The system model depends on the accurate characterization of the pump components. These include: membrane stiffness and mass (including the piezoelectric driver and electrical characteristics of the driver element), chamber fluid inertance and capacitance, valve resistance and inertance, and load capacitance, inertance, and resistance.

The characteristic parameters of individual pump components could not be independently determined experimentally in a complete pump. Numerical values for these characteristics were obtained by modeling each individual component. These component models were verified experimentally with a re-assembleable test fixture (RTF) that allowed substitution of individual components of the micropump. The RTF was designed to enable the use of different combinations of membranes, pump chambers, and inlet/outlet connections, with or without valves.

In addition to the RTF, two prototype pump designs were studied to better understand how various parameters affect pump performance. The two designs were termed “stiff” and “flexible”, and consisted of pump chamber diameters of 6 and 10 mm, Pyrex cover plate thicknesses of 500 and 150 μm , and piezoelectric driver element diameters of 3.8 and 6 mm, respectively.

METHODS

Fabrication

Pump chambers and valves were etched on silicon wafers using a Reactive Ion Etching (RIE) process to achieve precise control over the final etched shape in the valve regions. The micropumps had anodically bonded Pyrex membranes sealing the pump chamber and valves. Additional details are given in a previous publication (Forster et al, 1995). All silicon/Pyrex assemblies were mounted on steel or aluminum backing plates, (using Crytalbond 509, Aremco Products, Inc.).

The RTF consisted of a number of independent components built up around a silicon pump chip. Membranes of stainless steel or brass shim stock (127 μm thick) were used. A 5 mm diameter (190 μm thick) piezoelectric disk (PZT) was bonded to the membrane with conductive silver epoxy. Pump bodies were machined from 6.25 mm thick Plexiglas with a 10 mm diameter hole for the pump chamber. Inlet and outlet holes, as needed (depending on the property being tested), were drilled in the plexiglas and #18 gauge blunt tip needles were inserted and bonded in place. The membrane, pump body, and etched pump chip were pressed together by an outer assembly. The Plexiglas acted as its own gasket.

Linear System Model

A linear system model was developed using the RTF for experimental determination of individual system components. The circuit diagram was developed in pressure and flow units as shown in Fig. 2. The leftmost loop included the mechanical and electrical elements of the membrane as well as the chamber hydraulic elements. The applied pressure was $k f_e V / (\gamma A)$, the membrane inertance was $m / (\gamma A)^2$, and the membrane capacitance was $(\gamma A)^2 / k$. The two circuit branches on the right side represented the hydraulic elements of the input and output valves and tubes.

The system model was represented by a set of five governing equations. The force applied to the system by the PZT equaled the mechanical and pressure forces on the membrane.

$$k f_e V = m \frac{d\dot{W}_c}{dt} + k \int \dot{W}_c dt + \gamma A P \quad (1)$$

The pressure on the membrane was reduced by the inertance of the fluid in the chamber.

$$P = I_c \frac{dQ_c}{dt} + P_c \quad (2)$$

The chamber pressure depended on the capacitance of the chamber and the chamber flow rate (ie. volume rate swept by the membrane minus the inlet and outlet flows).

$$P_c = \frac{1}{C_c} \int Q_c - Q_i - Q_o dt \quad (3)$$

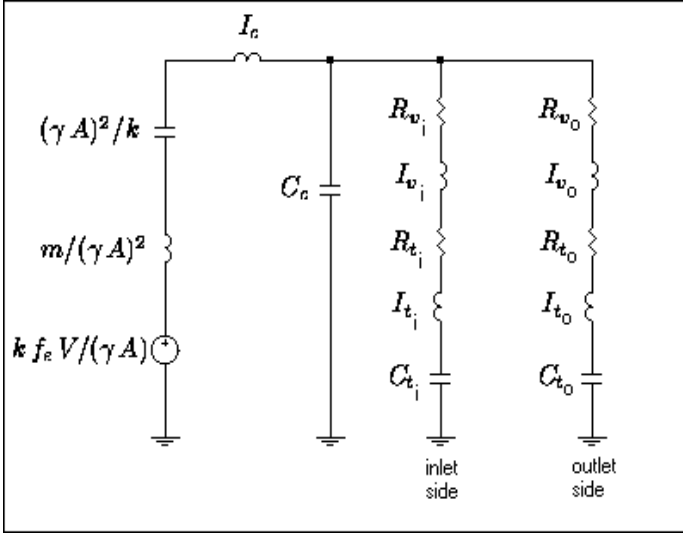


FIGURE 2: CIRCUIT DIAGRAM FOR THE LINEAR SYSTEM MODEL.

The final two equations represent the pressure drops across the valve and tubing in the inlet or outlet path. The same equation was used for both inlet and outlet, matching the experimental conditions. For example, the pump chamber pressure equals the sum of the pressure drops in the outlet path.

$$P_c = (R_v + R_t) Q_o + (I_v + I_t) \frac{dQ_o}{dt} + \frac{1}{C_t} \int Q_o dt \quad (4)$$

The key step used to develop a linearized set of equations to determine the frequency response of the system was to set the valve resistance and inductance for each valve flow direction to an average value. The resulting equations were then solved in the frequency domain assuming steady-state harmonic behavior for the applied voltage and the output quantities of interest. System response functions for the output parameters P_c , W_c , Q_c , and Q_o , relative to a unit input voltage, were determined as a function of frequency using Maple (Waterloo Maple Software). Numerical results were obtained with MatLab (The MathWorks, Inc.).

Component Models

To provide the parameters for the system model, individual pump component models were developed. The membrane was modeled as a bimetal disk with differential expansion, surrounded by an annular disk with fixed support on its outer periphery (Roark and Young, 1975, Table 24, Cases: 1e, 2e, 5e, 10a, 13a, and 15a). The deflection per volt, f_e , was calculated by replacing the thermal expansion coefficient with the voltage coefficient of the PZT. The

membrane stiffness, k , was determined from the predicted deflection to an applied pressure.

Unlike a piston, the membrane surface does not have a uniform amplitude due to the edges being fixed; thus the entire mass is not accelerated equally. The combined mass of the membrane and PZT disk was reduced to an effective mass by shape factors applied separately to the PZT disk and the membrane. The shape factors assumed a cosine shape for membrane deflection and integrated from center to outer radius of the membrane, or outer radius of the PZT.

$$\gamma = \frac{\text{effective mass}}{\text{actual mass}} = \frac{2\pi}{A} \int \frac{r}{2} \left(1 + \cos\left(\frac{r\pi}{r_o}\right) \right) dr \quad (5)$$

The effective mass, m , was then determined.

$$m = (\gamma m_{\text{actual}})_{\text{PZT}} + (\gamma m_{\text{actual}})_{\text{membrane}} \quad (6)$$

The chamber capacitance model contained terms representing the compressibility of the pumped liquid, the compressibility of air trapped in the pump chamber, and, for the RTF only (due to its flexible chamber material), the distension of the circumferential chamber walls.

$$C_c = \frac{A h_c}{K} + \frac{\hat{V}_a}{n P} + C_{\text{housing}} \quad (7)$$

The chamber inductance was calculated from the height and area of the pump chamber and the density of the fluid.

$$I_c = \frac{\rho h_c}{A} \quad (8)$$

The valve resistance model assumed laminar flow and integrated the resistance along the valve channels.

$$R_v = \frac{128 \mu L}{\pi d_H^4} = \frac{8 \mu}{\pi} \int \left(\frac{1}{h_v(x)} + \frac{1}{w_v(x)} \right)^4 dx \quad (9)$$

The valve inductance model considered the variation of valve channel width and height.

$$I_v = \rho \int \frac{dx}{h_v(x) w_v(x)} \quad (10)$$

Model Validation

Bench tests were performed to validate the preceding component model equations. All tests were performed with room temperature de-ionized water that was filtered to $0.2 \mu\text{m}$ and degassed by vacuum pump to approximately 2500 Pa. The RTF and the 10 mm diameter pumps were primed with methanol, electrically activated, and visually checked for bubbles. They were then flushed with filtered, degassed water. The same procedure was used for the 6 mm pump except it was primed with water instead of methanol,

which was incompatible with the adhesive used in its construction. While activated, the membrane displacement per volt was monitored, and additional degassed water was added until reduction in displacement per volt ceased, which was taken as an indication that air bubbles associated with filling had been removed. In the RTF, instantaneous cavity pressure was measured with a 2.1 mm diameter strain gage pressure transducer (Entran, Model EPI-411, Fairfield, NJ). Sine-wave voltage excitation was used for all tests.

The RTF was initially assembled as a PZT-activated membrane in free air. From this was obtained the membrane resonance, ω_n , and the displacement per volt, f_e .

$$f_e = \frac{\dot{W}_{c_a}}{\omega V} \quad (11)$$

The instantaneous pump membrane velocity was measured with a laser vibrometer (Polytec, Model OVF 302, Waldbronn Germany).

A water-filled pump chamber without valves or tubes was added to the RTF, and membrane velocity and chamber pressure were measured to verify the analytical membrane model's prediction of membrane stiffness, k .

$$k = \frac{\omega P_{c_w} \gamma A}{(\dot{W}_{c_a} - \dot{W}_{c_w})} \quad (12)$$

Both cases were excited at the same low frequency (50 Hz) at which inertial effects were determined to be negligible.

Additional verification of the membrane model was obtained by subjecting the stiff pump to various pressures and voltages, and measuring the membrane centerline deflection with a profilometer. The predictions for f_e were within 12% of the measured values at 100 V excitation and 50 Hz.

The chamber capacitance, C_c , was determined from the amplitudes of the instantaneous chamber pressure, P_c , and chamber volume, (ie. effective membrane area times deflection, $\gamma A \dot{W}_{c_w} / \omega$).

$$C_c = \frac{\gamma A}{\omega P_c} \dot{W}_{c_w} \quad (13)$$

These measurements were taken with the water-filled RTF with no inlet or outlet. The chamber capacitance model correlated with experimental results when an air volume, \hat{V}_a in Eqn. (7), equal to 0.1% of the chamber volume was used for the calculation of the capacitance apparently due to air trapped in the chamber.

The membrane mass and shape factor models were verified from the resonant frequency, ω_n , of the same RTF membrane in free air.

$$m = \frac{k}{\omega_n^2} \quad (14)$$

The chamber inertance model was verified from the resonance of the sealed, water-filled RTF pump chamber case described above.

$$I_c = \frac{k + \frac{A^2}{C_c}}{A^2 \omega_n^2} - \frac{m}{A^2} \quad (15)$$

For verification of the valve flow resistance model, the pressure drop across an entire pump (across both valves) was measured with a mercury manometer while flow was forced through the pump by a calibrated, constant-velocity, gear-driven infusion pump.

$$R_v = \frac{\Delta P}{Q} \quad (16)$$

The valve inertance model was not correlated due to the lack of a reliable experimental methodology.

RESULTS AND DISCUSSION

The results of the model validation confirmed the applicability of the pump component models, Eqs. (5-10), for determination of the system parameters in the linear system model Eqs. (1-4).

The linearized system transfer functions were used to determine the outlet volume flow rate Q_o , the membrane swept volume rate Q_c , the membrane centerline deflection W_c , and the pump chamber pressure P_c . Results for the stiff pump are shown in Fig. 3. Note that the difference between Q_c and Q_o at frequencies below the chamber resonance is 6 dB, which reflects that one-half of the flow generated by the membrane deflection is directed out the outlet valve of the pump. At frequencies above the chamber resonance these curves diverge as valve inertance reduces outlet flow, and more flow is taken up by the total chamber compliance due to the pumped liquid and trapped air. Also note that the higher frequency membrane resonance for Q_o has a significantly high amplitude, and if it was higher than the lower-frequency chamber resonance peak, it would correspond to the frequency at which the pump would produce its maximum output provided no cavitation occurs.

To validate the linear system model, the results of the model were compared to measured values in terms of membrane deflection W_c as a function of frequency for the stiff design. The results are shown in Fig. 4. Both the location of the membrane and chamber resonance peaks show good agreement. For the calculated curve all system parameters were determined from the correlated component models, except for the uncorrelated valve inertance model and the compliance due to air in the working fluid. Following the results of the RTF testing of the compliance model, a contribution to the chamber compliance due to an air volume equal to 0.1 percent of the chamber volume was chosen

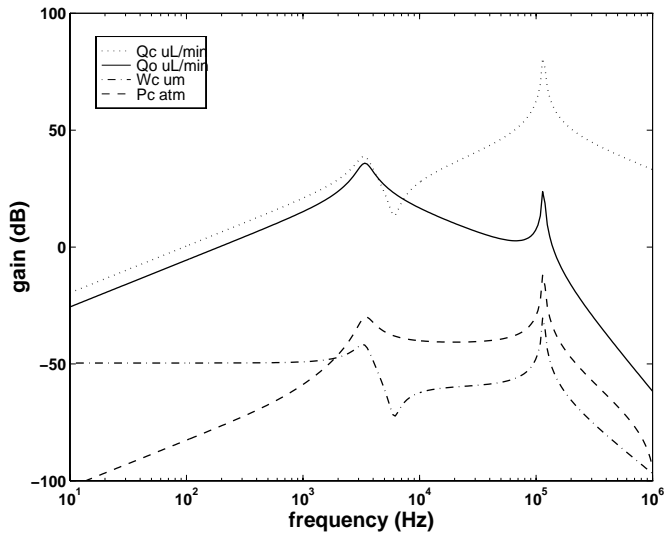


FIGURE 3: CALCULATED FREQUENCY RESPONSE FUNCTIONS FOR THE STIFF PUMP DESIGN SHOWING PEAK AMPLITUDES/VOLT OF MEMBRANE DISPLACEMENT W_c , CHAMBER FLOW RATE Q_c (RATE OF CHANGE OF CHAMBER VOLUME), OUTLET VALVE FLOW RATE Q_o , AND CHAMBER PRESSURE P_c . 0 dB = 1 unit/volt. THE DEVIATION OF Q_o FROM Q_c ABOVE THE FIRST RESONANCE IS DUE TO CAPACITANCE OF THE PUMP CHAMBER AND FLUID THEREIN. BELOW THE FIRST RESONANCE THE 6 dB DIFFERENCE IS ACCOUNTED FOR BY FLOW THROUGH THE INLET VALVE AND INTO THE CHAMBER COMPLIANCE.

to represent a realistic amount of air trapped in the pump chamber after degassing and filling, and the agreement between prediction and experiment is good. The exact volume of trapped air bubbles may be dependent on pump priming protocol.

The linearized system transfer functions were solved using parameters appropriate for each of the designs, the older flexible pump and the newer stiff pump. Figure 5 shows the system model predictions of output volume flow rate Q_o per unit input excitation voltage amplitude versus frequency. Each curve exhibits two resonance peaks. The higher frequency peak corresponds to the membrane resonance mode that is controlled primarily by the membrane mass and stiffness and chamber compliance. This peak exists even with no working fluid in the pump. The lower frequency resonance corresponds to a chamber resonance which is a strong function of chamber compliance and fluidic parameters of the valves and connected tubing.

The amplitude at the chamber resonance represents the largest amplitude over all frequencies considered. This point corresponds to the frequency at which an actual pump should produce the maximum output. The difference between the two designs at this optimum frequency is pre-

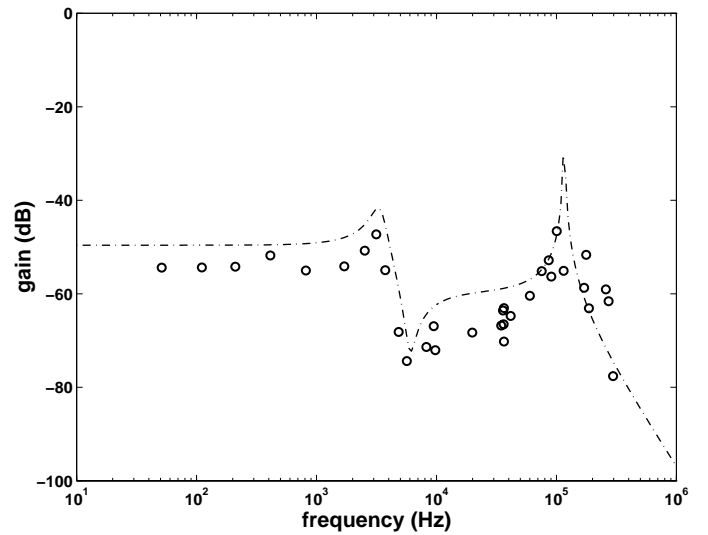


FIGURE 4: COMPARISON OF THE STIFF PUMP MODEL WITH EXPERIMENTAL DATA POINTS FOR PEAK CENTERLINE MEMBRANE DISPLACEMENT W_c . 0 dB = 1 μm per volt of PZT excitation.

dicted as approximately 25 dB. This agrees well with the maximum flow rates of 750 and 85 $\mu\text{l}/\text{min}$, or 19 dB, obtained experimentally as shown in Fig. 6, where performance tests of the older flexible pump and the newer stiff pump are compared. Performance curves for the stiff pump are given for three different excitation voltages. The performance curve for the flexible pump is only given at the highest voltage. However, at all voltage levels shown, the stiff pump performed significantly better than the flexible pump.

Figure 7 is a demonstration of how the linear frequency response model was used as a design tool. Shown in the figure is a parametric study showing how the outlet volume flow rate Q_o is affected by changes in Pyrex membrane thickness with all other pump parameters held constant. For a completely optimized design the size of the piezoelectric element would vary with membrane thickness, but the results shown demonstrate the potential for designing with the model.

CONCLUSIONS

For a given valve diodicity, an order-of-magnitude higher pump performance was achieved by selecting the characteristics of various pump components to increase the amplitude of the system response at one of the system resonance frequencies. A linear system model was developed to evaluate the effects of a complete set of pump components on performance over a range of frequencies that included all system resonance frequencies. Comparison with experimen-

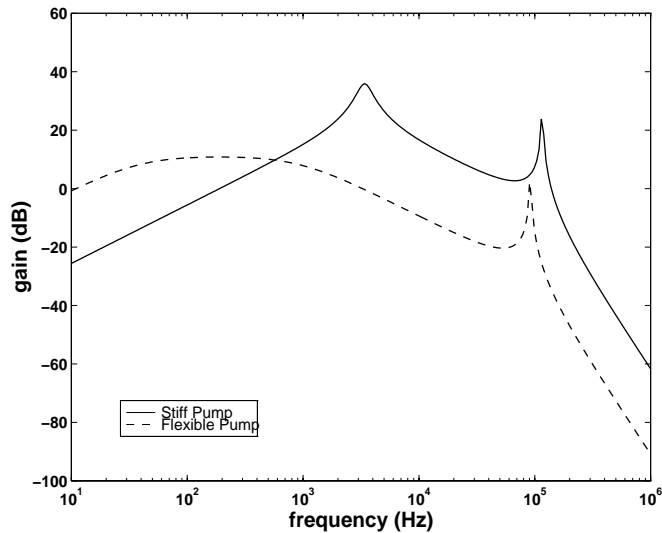


FIGURE 5: CALCULATED PEAK OUTLET FLOW RATE Q_o FOR THE STIFF PUMP COMPARED TO THE FLEXIBLE DESIGN. 0 dB = 1 μ l/min per volt of PZT excitation.

tal data showed good agreement between the system model and the dynamic response of a high performance prototype pump. Good agreement was also demonstrated when the model was used to predict the relative performance between flexible and stiff pump designs. Other strengths of a linear model include the ability to optimize pump performance and match it to desired performance levels. In addition, a linear system model can help determine operating performance under less than ideal conditions such as the presence of varying amounts of trapped air when pumping liquids.

ACKNOWLEDGEMENTS

This work was supported by the Washington Technology Center and MEMStek Products L.L.C. The Stanford University Nanofabrication Facility supplied deep RIE wafers of our designs.

REFERENCES

- Forster, F., Bardell, R., Afromowitz, M., Sharma, N., 1995, "Design, Fabrication and Testing of Fixed-Valve Micropumps," *Proceedings of the ASME Fluids Engineering Division, 1995 IMECE*, Vol.234, pp. 39-44.
- Gerlach, T. and Wurmus, H., 1995, "Working Principle and Performance of the Dynamic Micropump," *Sensors and Actuators A (Physical)*, Vol.50, no.1-2, pp. 135-140.
- Olsson, A., Enoksson, P., Stemme, G. and Stemme, E., 1995a, "A Valve-Less Planar Pump in Silicon," *The 8th International Conference on Solid-State Sensors and Actuators, and Eurosensors IX. Stockholm, June 25-29*, pp.

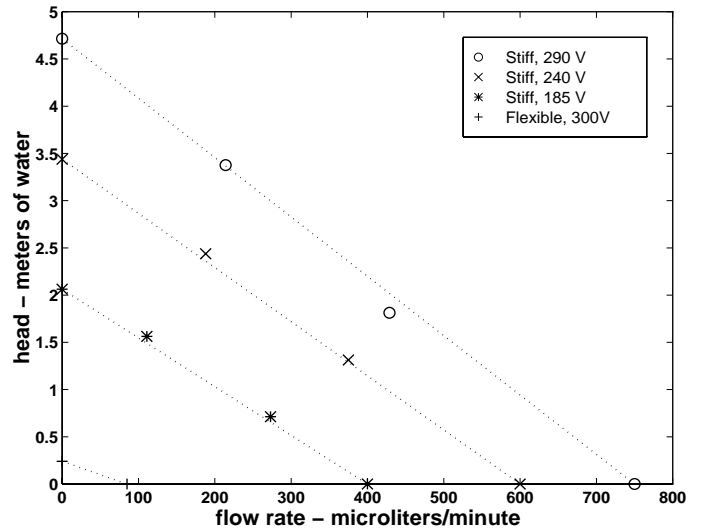


FIGURE 6: PERFORMANCE CURVES AT VARIOUS VOLTAGES FOR THE STIFF PUMP AND THE FLEXIBLE PUMP OPERATING AT THEIR RESPECTIVE RESONANCES. NOTE: DOTTED LINES DRAWN FOR CLARITY.

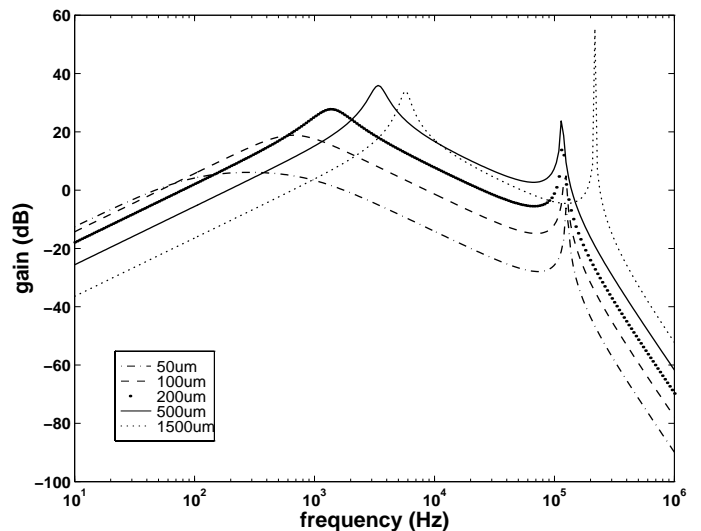


FIGURE 7: OPTIMIZATION STUDY FOR CHOOSING THE PYREX MEMBRANE THICKNESS FOR MAXIMUM OUTLET FLOW RATE Q_o . SHOWING THAT 500 μ m YIELDS THE MAXIMUM PERFORMANCE WHEN OTHER PUMP CHARACTERISTICS ARE HELD CONSTANT.

291-294.

Olsson, A., Stemme, G. and Stemme, E., 1995b, "A Valve-Less Planar Fluid Pump With Two Pump Chambers," *Sensors and Actuators A (Physical)*, Vol.46-47, pp. 549-556.

Olsson, A., Enoksson, P., Stemme, G. and Stemme, E., 1996, "An Improved Valve-Less Pump Fabricated Using Deep Reactive Ion Etching," *Proceedings of the IEEE, Ninth International Workshop on MEMS*, pp. 479-484.

Roark, R. and Young, W., 1975, *Formulas for Stress and Strain*, 5th edition, McGraw-Hill, New York, p.332.